An Electrodynamic Wheel Maglev Vehicle with a Passive U-Guideway

Colton Bruce
Laboratory of Magnetomechanical
Energy Conversion and Control
Portland State University
Portland, USA
bcolton@pdx.edu

Zhongkai Zheng Portland State University Portland, USA zhongkai@pdx.edu

Yew Tin Lee Portland State University Portland, USA yewtin@pdx.edu Jonathan Bird
Laboratory of Magnetomechanical
Energy Conversion and Control
Portland State University
Portland, USA
jonathan.bird@ieee.org

David Drake
Portland State University
Portland, USA
drakedav@pdx.edu

Jon Seeboth Portland State University Portland, USA jseeboth@pdx.edu Matthew Grubbs
Laboratory of Magnetomechanical
Energy Conversion and Control
Portland State University
Portland, USA
mgrubbs@pdx.edu

Anh Doane Portland State University Portland, USA anh32@pdx.edu

Abstract—This paper reports on the electromagnetic analysis and experimental testing of a newly invented six-degree of freedom electrodynamic wheel (EDW) magnetic levitation (maglev) vehicle that can stably levitate over a passive low-cost U-guideway. The U-guideway is composed of two sections of L-track aluminum sheet. Both a radial and an axial proof-of-principle EDW maglev vehicle has been built and experimentally tested. The EDW-maglev vehicle contains four one pole-pair diametric magnetized magnets that are driven using a low-cost motor and motor controller. No advanced controls are needed to provide basic stability. A 3-D transient finite element analysis model was used to study the 3-D forces created when the magnets are rotated over the aluminum L-track. The track design study showed that in addition to providing lateral recentering force the L-track can also be used to increases thrust and lift force.

Keywords— Eddy current, electrodynamic wheel, levitation, maglev

I. Introduction

Electrodynamic maglev vehicles use magnets to induce currents within conductive track material. The induced currents create an opposing field which can be utilized to create levitation, thrust and guidance forces. Electrodynamic maglev vehicles are being studied for use in ultra-high-speed ground transportation applications [1, 2] as well as in lower speed maglev vehicles [3]. Maglev vehicles offer trip times that are competitive with aircraft and can be powered with electricity created from renewable energy sources. Maglev vehicles' non-contact operation allows them to operate in harsh environments and operate on steep gradients. To lower the cost of maglev transportation the maglev track should be passive [4]. To accomplish this the maglev vehicle should be the initial field source, rather than the track.

Inducing current within a passive conductive track guideway by rotating magnets, rather than simply translating magnets, enables both a lift and thrust force to be simultaneously created [4]. The use of rotating magnets can create a relatively high lift-to-weight ratio [4]. In addition, when using magnets, the reactive field setup between the conductive track and magnet rotor is shielded from the driving motor.

In the past both radial [5, 6] and axial [8],[9],[10] EDW configurations, as illustrated in Fig. 1, have been studied. As the radial EDW's rolling motion is in the same direction as the travelling direction, the difference in the rotating magnet's circumferential speed relative to the translational speed can be controlled to give rise to both a thrust force, F_x , as well as a lift force, F_y . However, as the airgap is non-uniform only a small portion of the magnet material is utilized at any given time.

The axial rotor EDW has a uniform airgap with the flat track thereby leading to a higher lift-to-weight ratio, but no thrust force is then created. To additionally produce thrust the axial rotor can be tilted [7, 8], creating a non-uniform air-gap and asymmetric current flow, or the axial rotor can create thrust by using the track edge-effect [8],[9],[10], this also creates an asymmetric current flow. These axial EDW designs were first studied by Fujii *et al.* [8],[9],[10] and whilst they allow the axial EDW to create thrust, they will also significantly lower the lift force, reducing the benefits of the axial EDW relative to the radial configuration. More recently, Jung *et al* [11] and Qin *et al.* [12] have shown that by adding a rotor shield or adding supplemental rotor windings a rotor magnet field asymmetry can be created, reducing the field on one side of the magnet rotor; this can then give rise to a thrust

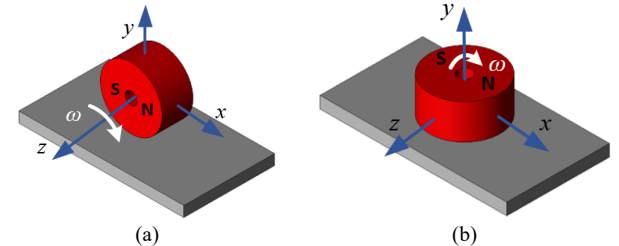


Fig. 1. An illustration of the (a) radial EDW and (b) axial EDW typology

force. But the use of a conductive rotor magnet shield will greatly increase loss and the addition of rotor windings around the magnets will significantly increase complexity as well as loss.

Both the radial and axial EDWs are laterally unstable when placed over a flat guideway sheet. If a single flat track is used, like shown in Fig. 1, the magnet rotors will try to minimize their energy by catastrophically exiting in the lateral, *z*-axis, direction. To intuitively understand this lateral instability, consider the case where a magnet is moving over a finite-width ladder track, as shown in Fig. 2. For illustrative purposes consider the influence of the mutual inductance between the track and moving magnet. In this case, the electromagnetic mutual energy in lumped-parameter form will be:

$$E_{m} = \frac{1}{2} M_{im}(x, z) i_{t}(x, z) i_{m} + \frac{1}{2} M_{mi}(x, z) i_{t}(x, z) i_{m}$$
 (1)

where i_g is the induced loop current and i_m = fictious magnet current that creates the magnet field. Since $M_{tm} = M_{mt}$ the energy in terms of mutual flux is:

$$E_m(x,z) = \Phi(x,z)i_m \tag{2}$$

where $\Phi = M_{tm}i_t$. The magnetic force acting on the guideway in the lateral z-axis direction can be obtained from the negative energy gradient: [13]

$$F_z = -\frac{\partial E_m}{\partial z} \tag{3}$$

Thus, assuming that the magnet source current is not changing and then substituting (2) into (3) the lateral force will be:

$$F_z = -i_m \frac{\partial \Phi}{\partial z} \tag{4}$$

From (4) it can be noted that the lateral force will depend on the gradient of the mutual flux. For the magnet guideway configuration shown in Fig. 2 the flux will be a maximum when the magnet is centered over the guideway and therefore the energy profile, E_m , as a function of the lateral position, z, and the resultant lateral force, F_z , will have the form shown in Fig. 3. Stability can never be assured as a lateral force will always be created to push the magnet off the guideway. This same analysis applies to the EDWs that are shown in Fig. 1.

To provide passive stability the maglev's magnets need to rest within a mutual energy minimum. One way to create a local energy minimum is to use a split-track guideway [14]. However, by splitting the track the currents are prevented from circulating below the maximum rotor field location and therefore the split-track greatly reduces the lift and thrust force. The amount of re-centering force is also relatively small and does not scale well with size. Lateral stability can also be created by using a curved track, like shown in [15], however, for track design the EDW does not create thrust and the use of any curved, or wrap-around track, greatly increase the guideway construction and operating cost. Since to enable vehicle lane changing the entire guideway must be moved.

It has also been proposed that active control could be used to create stability, by mechanically rotating the EDW's axis the EDW force direction can be constantly adjusted so as to enable the EDW to be maintained on a single flat guideway [16]. This approach has yet to be experimentally demonstrated but if the EDW rotation controls failed it would lead to a catastrophic crash (like with some aircrafts).

This paper studies a new type of L-track EDW typology as shown in Fig. 4. This paper shows that when two L-tracks are

combined to form a U-guideway an EDW-maglev vehicle can have 6-degrees-of-freedom stability. In this paper each EDW is composed of a simple one pole-pair diametrically magnetized rotor magnet. A higher number of EDW rotor pole-pairs could also be used, but to provide the lowest lift specific power (W/kg), as well as simplify the construction, the one pole-pair rotor was used. The ability of the one pole-pair radial EDW to operate with a near constant airgap, despite creating relatively high lift force ripple, is discussed in [17].

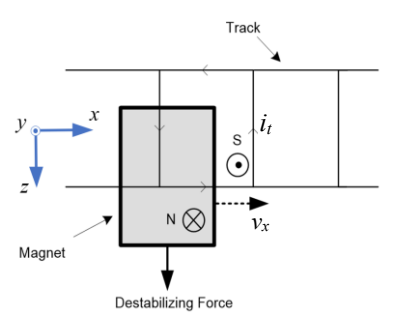


Fig. 2. Sketch of a magnet moving over a conductive guideway

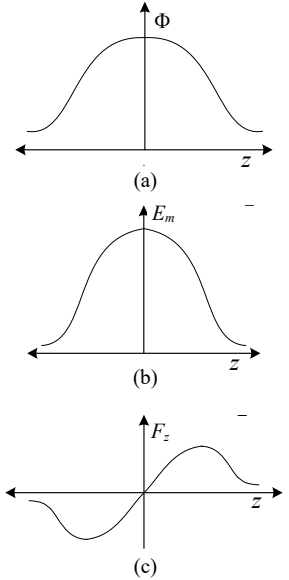


Fig. 3. Sketch of (a) the guideway mutual flux, Φ , seen by the track, (b) mutual energy, E_m , and (c) force, F_z

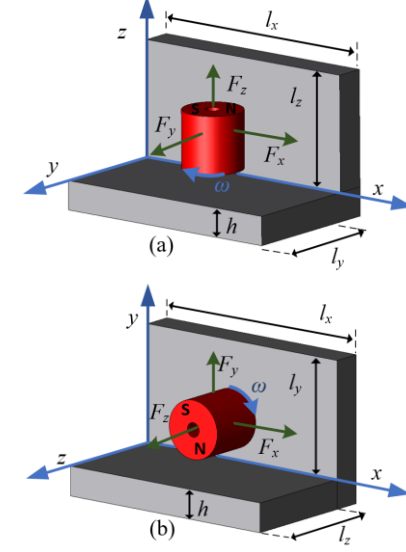


Fig. 4. (a) A 3-D persepctive view of a one pole-pair axial EDW over an L-track and (b) a radial EDW. The force components are also shown.

II. L-TRACK FORCE ANALYSIS

For this analysis the radial and axial EDW forces are defined using the coordinate axis with respect to the rotor axis shown in Fig. 4. A front-view of one radial EDW showing the offset length, z_g , and track height, l_y , definitions is shown in Fig. 5(a) and Fig. 5(b) shows the case when the track is flat, $l_y = 0$. To study how the track-side height and offset length effects force, the force on only one radial EDW was first studied.

Using the geometric parameters shown in Table I and Table II the forces created between the L-track and the rotating one-pole pair EDW were computed using a 3-D transient finite element analysis (FEA) model developed in JMAG. Fig. 6 shows a plot of the steady-state force components as a function of EDW rotor offset as well as track height. The forces were computed for the case when $\omega = 5000$ r/min and $(v_x, v_y, v_z) = (0,0,0)$. Fig. 6(a) shows that when the rotor is axially centered, $z_g = 6.35$ mm with $l_y = 0$, the axial force is zero. But when $l_y = 0$, the EDW has a negative stiffness, and any lateral offset will cause the lateral force to increase in the direction of motion, leading to the EDW exiting the track. When there is a vertical side height on the track, the side track creates an additional axial force, F_z , the direction of this force depends on the height of the side-track. Interestingly, as the track-side height increases the stiffness changes from a negative (unstable), to positive (stable) stiffness. For the geometry given, this occurs when the track-side height is $l_v >$ 10.9 mm; lateral force is then created that still pushes the rotor off the track, but only in the positive z-axis direction.

Fig. 6(b) and (c) show the effect of rotor offset on the lift force and thrust force, respectively. When $l_y = 0$ the lift and thrust force do not perceptively change with rotor offset, this is only because the rotor is not sufficiently close to the track edge. The increase in track-side height increases the lift and thrust force. When the rotor is at the minimum offset of $z_t = 2$ mm the lift force increases from 6 N to 9.6N, a 60% increase, whilst the thrust force increased from 4.3 N to 7.5 N, a 74% increase. Therefore, while the presence of the side-track increases loss, it also significantly increases the lift-to-weight ratio as well as thrust force.

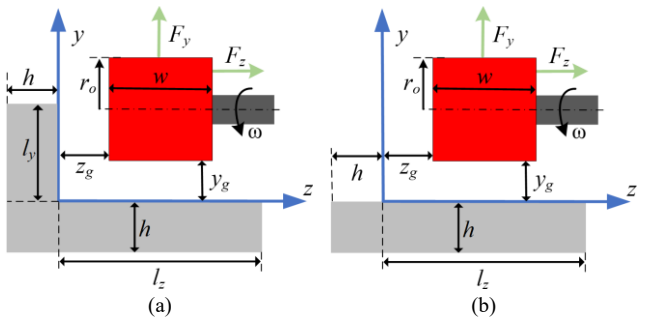


Fig. 5. (a) A front view of the EDW showing the EDW having a lateral offset distance z_g from the side-track and and airgap height y_g . The side track length is defined has l_y . Note when $l_y = 0$ the side hight is zero as shown in (b) and in this case at $z_g = 6.35$ mm the EDW is centered over the flat track.

TABLE I. SIMULATION AND EXPERIMENTAL MATERIAL PROPERTIES

Parameter	Value	Units
Track conductivity, σ	2.5×10 ⁷	S/m
Magnet residual flux density, B_{rm}	1.32	T
Magnet relative permeability, μ_r	1.055	-
Magnet mass, m	0.0905	kg

TABLE II. SIMULATION SWEEP PARAMETERS AND EXPERIMENTAL VALUES

Parameter	FEA simulation value [mm]	Experimental value [mm]
Rotor outer radius, r_o	12.7	12.7
Rotor inner radius, r_i	3.175	3.175
Rotor width, w	$2r_o$	$2r_o$
Radial airgap, yg	7	varied
Track thickness, h	12.7	6.35
Track length, l_x	100	2438.4
Track width, $l_z = 2.5w$	50.8	57.15
Rotor offset, z_g	[2,1,11]	0
Track-side height, l_y	3.175 [0,1,6]	31.75

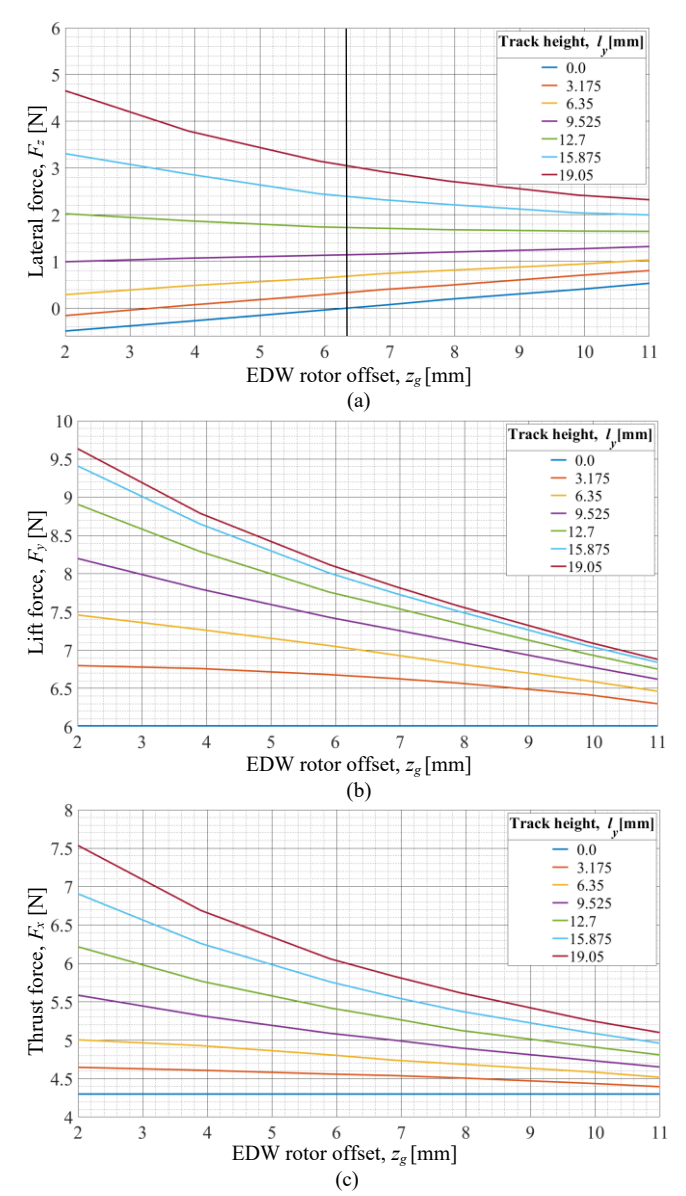


Fig. 6. (a) 3-D FEA calcuated lateral force, F_z , a a function of EDW rotor offset, z_g , and track-side height, l_y , when the angular speed is $\omega = 5000$ r/min. (b) lift force, and (c) thrust force. The geometric and material values shown in Table I and Table II were used.

III. EDW VEHICLE WITH A U-GUIDEWAY

To create a recentering force regardless of axial position, a U-track guideway was investigated. A front-view of a U-track EDW maglev that contains radial EDWs is shown in Fig. 7. Also sketched in Fig. 7 are the brushless DC motors and the vehicle mounts. In the following radial EDW analysis, the vertical height of the EDWs is fixed at $y_g = 7$ mm and the vehicle is assumed to be laterally centered when:

$$z_{g1} = z_{g2} = z_{g3} = z_{g4} = 6.35 \,\mathrm{mm}$$
 (5)

where z_{g1} and z_{g2} are the distances from the EDW and leftside track and z_{g3} and z_{g4} are the distances from the right-side track. Only the z_{g1} and z_{g3} distances are shown in the frontview in Fig. 7. When (5) is satisfied the net lateral force is zero. The 3-D FEA calculated change in lateral force as well as lift and thrust as the vehicle is laterally offset is shown in Fig. 8. Also shown is the change in the force with respect to

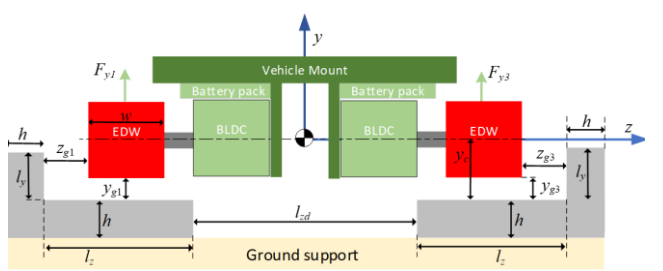
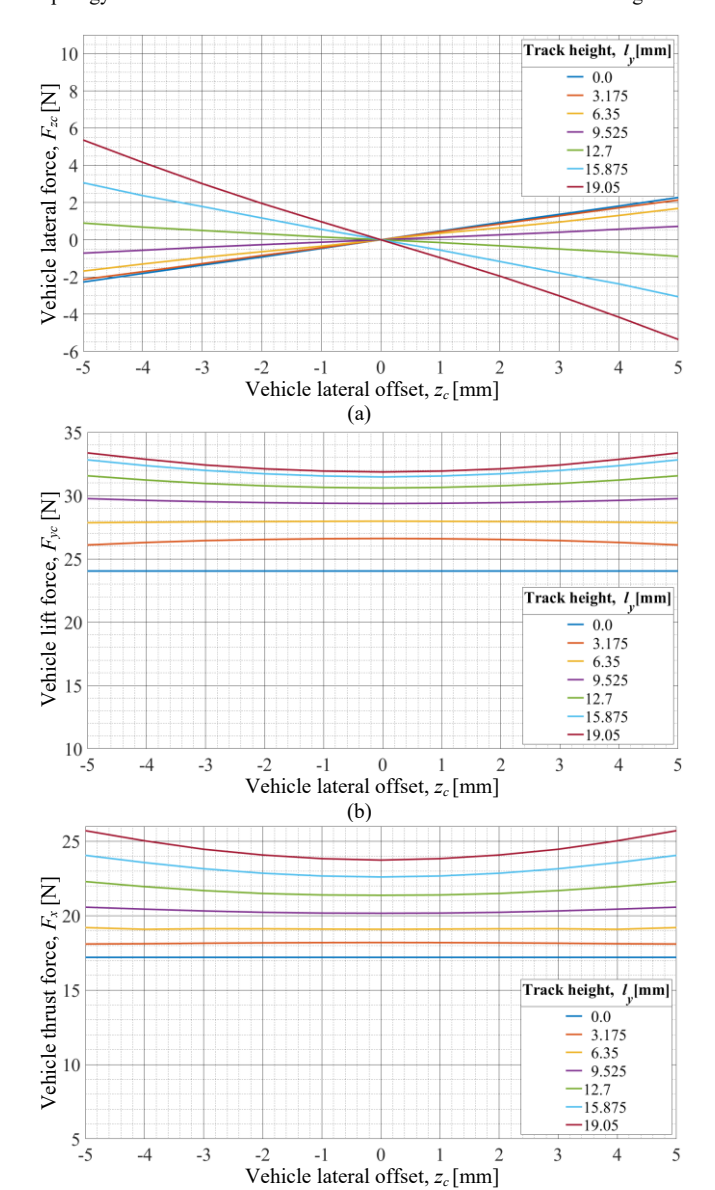


Fig. 7. A front-view of the centered radial EDW-vehicle with the U-track topology. Also shown are the two BLDC motors used to rotate the magnets.



(c) Fig. 8. (a) EDW-maglev vehicle lateral force, F_{zc} , (b) lift force, F_{yc} , and (c) thrust force, F_{xc} , as a function of track-side height, l_y , and lateral offset, z_c . FEA calculation performed when $\omega = 5000$ r/min and $y_g = 7$ mm.

track-side height, l_y . The vehicle lateral offset is defined as

$$z_c = (z_{g1} + z_{g2} - z_{g3} - z_{g4})/4 (6)$$

The EDW rotor's thrust and lift force add when the rotors are offset, and the vehicle lateral force is defined as:

$$F_{zc}(z_c) = F_{z1}(z_{g1}) + F_{z2}(z_{g2}) - F_{z3}(z_{g3}) - F_{z4}(z_{g4})$$
 (7

The EDW-vehicle recentering axial force is highly linear and the calculated axial stability occurs when $l_y \ge 10.9$ mm. This cross-over length can be more clearly seen in Fig. 9 in which the total axial force at the offset position $z_c = -5$ mm is shown.

Fig. 8(b) and (c) show how the thrust and lift force increases as the track-side height increases, these force components are almost decoupled from the lateral offset. Fig. 10(a) shows that the thrust and lift force peak as the track height is increased. Based on the simulation conditions and geometry used in this paper the track height that gave the peak thrust and peak lift occured when $l_{yx} = y_g + 1.95r_o = 31.75$ mm and $l_{yy} = y_g + 1.2r_o = 22.23$ mm, respectively. To maximize the lift force the side track-height should be lower than the EDW diameter.

The increase in lift as the track-side height increases improves the lift-to-weight ratio, this improvement is shown in Fig. 10(b). The lift-to-weight ratio is defined by

$$L_{w} = \frac{F_{y}}{mg} \tag{8}$$

where m = magnet mass. The lift force is created from the currents induced on the track edge, pushing the EDW upwards, off the track edge. This increase in lift comes at an increase in lift specific power (W/kg), as shown in Fig. 10(c). The lift specific power is defined as

$$S_w(v_x) = \frac{P_L}{F_y / g} \qquad [W/kg]$$
 (9)

where P_L = total electrical track loss. It should be noted that the lift specific power is relatively high, this is because of the small diameter used as well as the high angular speed selected for the force analysis.

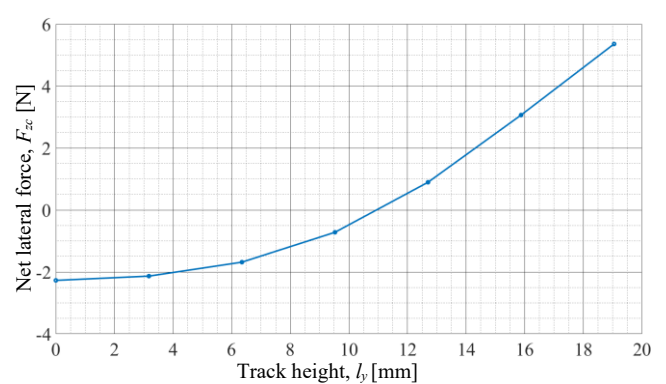


Fig. 9. Four rotor radial EDW-maglev vehicle lateral force vs. track height, l_y , when the EDW rotor is offset by $z_c = -5$ mm and when the angular speed is $\omega = 5000$ r/min. and the air-gap is maintained at $y_e = 7$ mm.

IV. PROOF-OF PRINCIPLE EXPERIMENTAL EDW-VEHICLE

A proof-of-principle axial EDW-maglev vehicle as well as a radial EDW-maglev vehicle were built and initially tested. The two maglev vehicles are shown in Fig. 11 and the geometric parameters used in these experimental setups are shown in Table I and II. The axial and radial vehicle mass is

 $m_a = 1.32$ kg and $m_r = 1.82$ kg, respectively. The radial EDW is heavier due to the vehicle also containing four height laser sensors. The vehicles were wirelessly operated and can linearly travel along the U-guideway. The stability at a range of

different operating speeds as well as the vehicle heights is currently being measured using laser sensors.

Past studies [3] have indicated that maglev vehicles that use translationally moving magnets to create electrodynamic levitation can experience instability at different operating speeds. As the EDW vehicle has a slip speed, as well as translational speed, and these two speeds can be independently changed it is believed that the EDW vehicle could more easily overcome instability induced at particular operating speeds. These dynamic aspects are still being investigated.

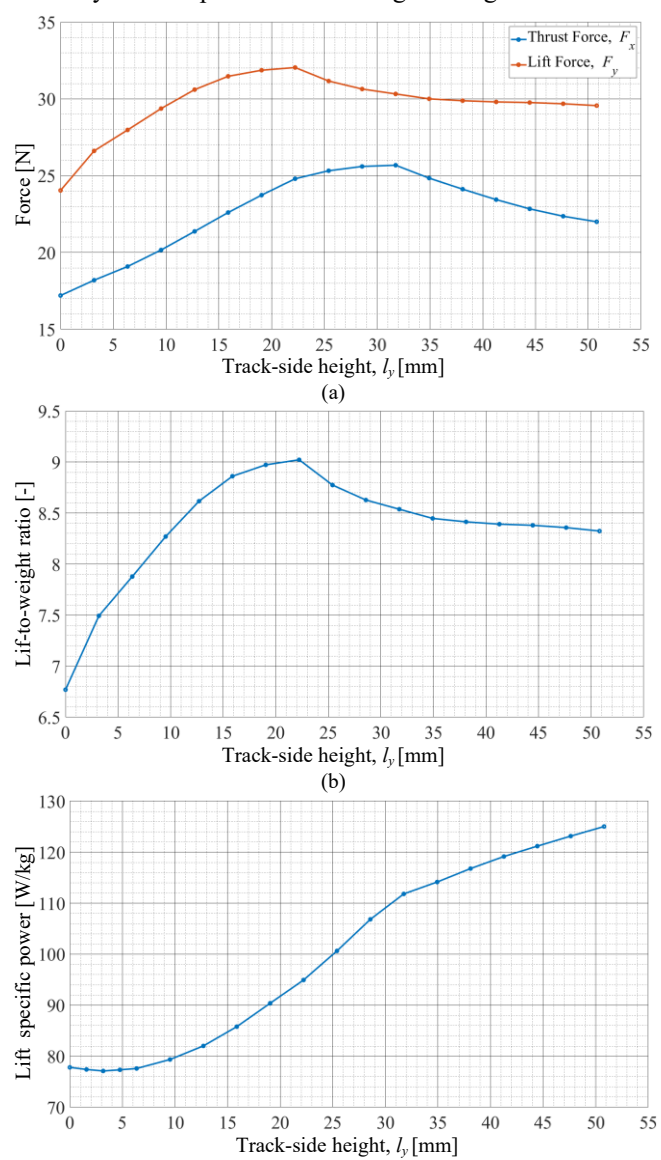


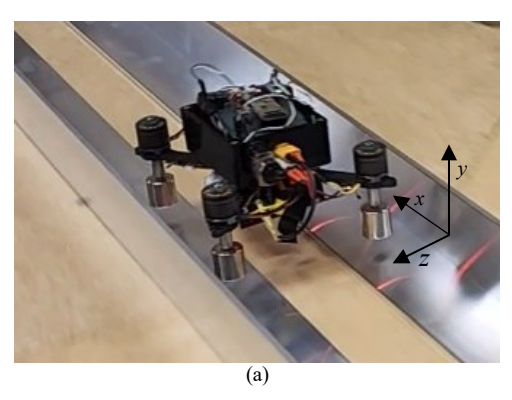
Fig. 10. (a) Four rotor radial EDW-maglev thrust and lift force, (b) lift-to-weight ratio, and (b) lift specific power as a function of track-side height, l_y , when the EDW-maglev vehicle is not offset, $z_c = 0$ mm, the air-gap is $y_g = 7$ mm, and the angular speed is $\omega = 5000$ r/min.

(c)

CONCLUSIONS

The paper has presented a new type of radial and axial EDW maglev vehicle that can stably levitate and translate above a low-cost U-guideway. The recentering forces that

give rise to lateral stabilty were investigated using a 3-D FEA model. The EDW-maglev vehicle's stability was confirmed through the experimental testing of proof-of-principle radial and axial EDW-maglev vehicles. It should be noted that to verify stability over a full range of speeds further testing and height and motion measurements are being conducted. The use of the EDW allows force corrections to be actively achieved using the vehicle and not the track. The EDW-maglev vehicle as well as the guideway can be constructed using low-cost, and off-the-shelf, components.



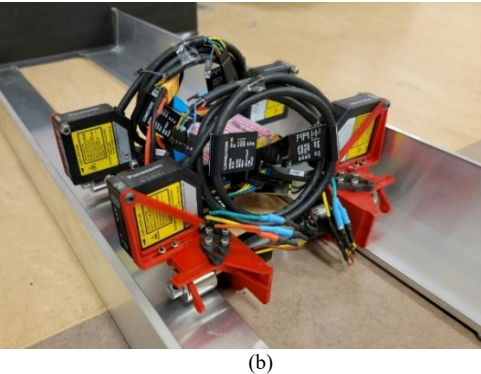


Fig. 11. (a) A four axial EDW proof-of-principle maglev vehicle travelling along a 11-meter length L-track and (b) the four-rotor radial rotor EDW maglev vehicle. The rotors are wirelessly controlled and driven by brushless DC motors

ACKNOWLEDGMENT

The authors would like to thank the JMAG Corporation for the use of their FEA software. This material is based upon work supported by the National Science Foundation under grant number 1810489.

REFERENCES

- [1] J. K. Nøland, "Prospects and Challenges of the Hyperloop Transportation System: A Systematic Technology Review," in *IEEE Access*, vol. 9, pp. 28439-28458, 2021.
- [2] M. Flankl, T. Wellerdieck, A. Tüysüz, and J. W. Kolar, "Scaling laws for the Electrodynamic Suspension in High-Speed Transportation," in IET Electric Power Applications, vol. 12, no. 3, pp. 357-364, 2018.
- [3] D. M. Rote and Y. Cai, "Review of Dynamic Stability of Repulsive-Force Maglev Suspension Systems," in *IEEE Transactions on Magnetics*, vol. 38, no. 2, pp. 1383-1390, March 2002.
- [4] J. Z. Bird, "A Review of Integrated Propulsion, Suspension and Guidance Passive Guideway Maglev Technologies," in 2019 12th International Symposium on Linear Drives for Industry Applications (LDIA), 1-3 July 2019, pp. 1-6.
- [5] H. Zhang, K. Kails, P. Machura, and M. Mueller, "Conceptual Design of Electrodynamic Wheels Based on HTS Halbach Array Magnets," in *IEEE Transactions on Applied Superconductivity*, vol. 31, no. 5, pp. 1-6, 2021.

- [6] J. Wright and J. Z. Bird, "Analytic Damping and Stiffness Analysis for a 4-DOF Electrodynamic Wheel Maglev Vehicle," in 2018 XIII International Conference on Electrical Machines (ICEM), 3-6 Sept. 2018, pp. 555-561.
- [7] D. G. Henderson *et al.*, "Hoverboard," US20150175031A1, June. 25, 2015.
- [8] N. Fujii, K. Naotsuka, K. Ogawa, and T. Matsumoto, "Basic Characteristics of Magnet Wheels with Rotating Permanent Magnets," *Industry Applications Conference*, 1994, vol. 1, pp. 203-209.
- [9] K. Ogawa, Y. Horiuchi, and N. Fujii, "Calculation of Electromagnetic Forces for Magnet Wheels," in *IEEE Transactions on Magnetics*, vol. 33, no. 2, pp. 2069-2072, March 1997.
- [10] N. Fujii, G. Hayashi, and Y. Sakamoto, "Characteristics of magnetic lift, propulsion and guidance by using magnet wheels with rotating permanent magnets," in *Industrial Applications Conference* Rome, Italy, Oct. 2000, pp. 257-262.
- [11] K. S. Jung, "Spatial transfer of conductive plate through decoupling of two axial electrodynamic forces generated by magnet wheel," *Mechatronics*, vol. 23, no. 8, pp. 1044-1050, 2013.
- [12] W. Qin, M. Yuhua, L. Gang, W. Fuyao, S. Chengrui, and Z. Jielong, "Investigation of Asymmetric Axial-flux Hybrid Excited

- Electrodynamic Wheels for Maglev Transportation," in 2021 IEEE Energy Conversion Congress and Exposition (ECCE), 10-14 Oct. 2021 2021, pp. 3753-3758
- [13] H. E. Knoepfel, Magnetic fields: A Comprehensive Theoretical Treatise for Practical Use. New York: John Wiley & Sons, 2000.
- [14] J. Bird and T. A. Lipo, "Modeling the 3-D Rotational and Translational Motion of a Halbach Rotor Above a Split-Sheet Guideway," in *IEEE Transactions on Magnetics*, vol. 45, no. 9, pp. 3233-3242, Sept. 2009.
- [15] J. Duan, W. Zhang, S. Xiao, K. Zhang, and J. K. Sykulski, "Investigation of the Characteristics of the Electrodynamic Wheel Suspension Device With Two-DOF Motion," in *IEEE Transactions* on *Plasma Science*, vol. 48, no. 6, pp. 2274-2279, 2020
- [16] J. Bird, "An investigation into the use of electrodynamic wheels for high-speed ground transportation," Ph.D. Thesis, Electrical and Computer Engineering, University of Wisconsin-Madison, Madison, WI, 2007.
- [17] C. Bruce, M. Grubbs, and J. Z. Bird, "Dynamic Lift Force Analysis of a One-Pole-Pair Electrodynamic Wheel Maglev Vehicle," Submitted to IEEE Trans. Magnetics 2022.